



## Ecosystem responses to elevated CO<sub>2</sub> using airborne remote sensing at Mammoth Mountain, California

Kerry Cawse-Nicholson<sup>1</sup>, Joshua B. Fisher<sup>1</sup>, Caroline A. Famiglietti<sup>1</sup>, Amy Braverman<sup>1</sup>,  
5 Florian M. Schwandner<sup>1,2</sup>, Jennifer L. Lewicki<sup>3</sup>, Philip A. Townsend<sup>4</sup>, David S. Schimel<sup>1</sup>,  
Ryan Pavlick<sup>1</sup>, Kathryn J. Bormann<sup>1</sup>, Antonio Ferraz<sup>1</sup>, Emily L. Kang<sup>5</sup>, Pulong Ma<sup>5</sup>, Robert  
R. Bogue<sup>1</sup>, Thomas Youmans<sup>1</sup>, David C. Pieri<sup>1</sup>

<sup>1</sup>Jet Propulsion Laboratory, California Institute of Technology, Pasadena, CA, USA

<sup>2</sup>Joint Institute for Regional Earth System Science and Engineering, University of California  
10 Los Angeles, Los Angeles, CA, USA

<sup>3</sup>United States Geological Survey, Menlo Park, CA, USA

<sup>4</sup>University of Wisconsin-Madison, Madison, WI, USA

<sup>5</sup>University of Cincinnati, Cincinnati, OH, USA

Correspondence to: Kerry Cawse-Nicholson, [kcawseni@jpl.nasa.gov](mailto:kcawseni@jpl.nasa.gov)

15 **Abstract.** We present an exploratory study examining the use of airborne remote sensing  
observations to detect ecological responses to elevated CO<sub>2</sub> emissions from active volcanic  
systems. To evaluate these ecosystem responses, existing spectroscopic, thermal, and lidar  
data acquired over forest ecosystems on Mammoth Mountain volcano, California, were  
exploited, along with *in situ* measurements of volcanic soil CO<sub>2</sub> fluxes. The elevated CO<sub>2</sub>  
20 response was used to statistically model ecosystem structure, composition and function,  
evaluated via data products including biomass, plant foliar traits and vegetation indices, and  
evapotranspiration (ET). Using regression ensemble models, we found that soil CO<sub>2</sub> flux was  
a significant predictor for ecological variables, including Normalized Vegetation Difference  
Index (NDVI), canopy nitrogen, ET, and biomass. Additionally, the relationships between  
25 ecological variables changed with increasingly elevated (volcanically influenced) over non-  
volcanic “background” soil CO<sub>2</sub> fluxes, suggesting a shift in coupling/decoupling among  
ecosystem structure, composition, and function synergies. For example, ET and biomass  
were significantly correlated for areas without elevated CO<sub>2</sub> flux, but decoupled with  
elevated CO<sub>2</sub> flux. This study demonstrates that a) volcanic systems show great potential as a  
30 means to study the properties of ecosystems and their responses to elevated CO<sub>2</sub> emissions  
and b) these ecosystem responses are measureable using a suite of airborne remotely sensed  
data.



## 1 Introduction

Terrestrial ecosystems have consistently taken up carbon over the past century, in excess or balancing losses due to deforestation and land use change, and this sink has grown with time (Le Quéré et al., 2016; Schimel et al., 2015). Much debate, however, has centred on the drivers of this uptake. Suggested mechanisms include nitrogen deposition (Peterson and Melillo, 1985), land use (Schimel, 1995), and the direct effects of carbon dioxide on plant growth (Norby et al., 2016). The last, which proposes that increased atmospheric CO<sub>2</sub> yields increased photosynthetic rates, is both the most probable and the most controversial. Although a multitude of experiments have shown positive photosynthetic responses to increased CO<sub>2</sub> consistent with the observed growth in the terrestrial sink (Drake et al., 1997), many ecologists have argued that plant growth in intact ecosystems is limited by water, light or nutrients, rather than CO<sub>2</sub> (Körner, 2006; McGuire et al., 1995).

The Free-Air Carbon Enrichment (FACE) experiments, introduced in the 1990s, allow for CO<sub>2</sub> fertilization of intact ecosystems by creating controlled fumigation conditions without the use of a growth chamber (Lewin et al., 1994). These studies have shown some consistent responses indicative of enhanced growth (Norby et al., 2016), as well as other physiological, morphological and ecosystem consequences, but also suffer from several structural deficiencies. Perhaps most notably, only short-term study periods are feasible; the longest-running experiment spanned only a decade, while atmospheric CO<sub>2</sub> has been steadily rising for more than an order of magnitude longer than that duration. FACE can thus elucidate physiological responses to elevated CO<sub>2</sub>, but cannot unshroud slower processes like plant acclimation, shifts in species dominance induced by CO<sub>2</sub>, or other long-term mechanisms mediated by changes to soil organic matter and nutrients. Additionally, because FACE experiments are vastly expensive to construct and operate, they tend to be small in scale, limited in replicability, and homogeneous in species, soils and landscapes.

As a result of limited empirical evidence for the strength of CO<sub>2</sub> fertilization effects, global carbon cycle models disagree about the significance of their associated impacts. Some models show very large CO<sub>2</sub> effects, while others indicate a smaller or saturating effect (Kolby Smith et al., 2015). Because future predicted fossil carbon uptake is highly dependent on the strength of the simulated CO<sub>2</sub> fertilization, any constraints on the long-term effect of elevated CO<sub>2</sub> on ecosystems would be valuable in reducing uncertainty in coupled carbon-climate models (Friedlingstein et al., 2014).

Diffuse volcanic CO<sub>2</sub> emissions result from the degassing of magma beneath volcanoes and offer a continuous natural experiment to study vegetation responses to elevated CO<sub>2</sub> that is expansive in both space and time. These surface discharges yield broad atmospheric



enhancements that transport CO<sub>2</sub> downwind (Kerrick, 2001), resulting in swaths of variably affected plants whose periods of exposure can be over hundreds of years (Cook et al., 2001). Because volcanic CO<sub>2</sub> emissions are a vital part of the global carbon cycle (Mason et al., 2017; Schwandner et al., 2017) and have been monitored worldwide for decades (Boudoire et al. 2017; Camarda et al., 2012; Perez et al., 2011; Gerlach, 1991), the rate and spatial  
5 distribution of these fluxes are well-understood due to an abundance of field surveys in many volcanic systems (e.g. Hernández et al., 1998; Cardellini et al., 2003; Werner and Brantley, 2003; Giammanco et al., 2007; Lewicki et al., 2014a). Although the spatial distributions of CO<sub>2</sub> emissions within tree kill areas have been well mapped (Pickles et al., 2001; Werner and  
10 Brantley, 2003; List et al., 2005, and others), linking CO<sub>2</sub> measurements to vegetation responses along a spatially diffuse CO<sub>2</sub> degassing continuum is a natural yet underutilized opportunity for studying the effects of elevated CO<sub>2</sub> on plants (Schwandner et al., 2004). Furthermore, many CO<sub>2</sub> emissions in volcanic systems have been ongoing for decades or centuries, thus allowing for the observation of equilibrium, long-term ecosystem responses  
15 after transient and acclimational responses have passed.

While FACE experiments may demonstrate ecological responses to increased CO<sub>2</sub> at the outset of elevation, studies in volcanic basins can do the same on super-century scales. However, because volcanic emissions can affect entire landscapes differentially depending on  
20 the flow of the gas, they require new and innovative techniques for analysis. Remote sensing observations allow for detailed measurements across a wide spatial extent that can be used to analyse ecological indicators of CO<sub>2</sub> effects.

Here, we present an exploratory study examining the use of airborne remote sensing data to  
25 detect ecological responses to elevated volcanic CO<sub>2</sub> emissions. We leveraged existing data over Mammoth Mountain, California – a much-studied volcano that has been passively emitting CO<sub>2</sub> at high concentrations through faults and fissures on its flanks, measured systematically since a large earthquake swarm in 1989 (Farrar et al., 1995; Lewicki et al.,  
30 2014b, b; Werner et al., 2014). Figure 1 shows that the elevated soil CO<sub>2</sub> fluxes, measured by the USGS over a span of two decades, far exceed the atmospheric CO<sub>2</sub> measured by a flux tower at the same site. We developed a statistical framework for examining the relationships between field measurements of soil CO<sub>2</sub> emissions into the air below the forest canopy and a suite of remotely sensed ecological variables. In this investigation, we aim to: (i) evaluate the  
35 viability of using a passively degassing volcanic system to study the properties of ecosystems; (ii) assess the detectability of ecological responses to elevated soil CO<sub>2</sub> emissions via airborne data alone; and (iii) present key lessons enabling future studies to extend our framework to other biomes. This methodology can applied to any site that is exposed to elevated CO<sub>2</sub>.



## 2 Methods

### 2.1 Data

Airborne remote sensing data from multiple sources have been acquired over Mammoth Mountain, California, USA, providing a substantial means to assess ecosystem structure (products derived from lidar, such as canopy height and biomass), composition (products derived from spectral data, such as vegetation indices and plant foliar traits), and function (data products derived from thermal data, such as evapotranspiration). Figure 2 illustrates several of the different products used in this study, highlighting the diversity of data sources and spatial resolutions.

Mammoth mountain is an upper montane forest ecosystem, characterised by abundant *Pinus contorta* (lodgepole pine), and also by mature stands of *Abies magnifica* (red fir), *Pinus jeffreyi* (Jeffrey pine), *Pinus albicaulis* (whitebark pine), and *Juniperus occidentalis* (western juniper) (Potter, 1998). The elevation of our study areas ranged from 2700 to 2950 m. Tree-kill soils are immature High Sierra soils formed from granite, pumice, rhyolite, and obsidian parent materials (McGee and Gerlach, 1998).

#### 2.1.1 Ground measurements

We investigated soil CO<sub>2</sub> fluxes within five actively degassing areas on Mammoth Mountain documented by Werner et al. (2014) in 2011 and 2012, which represents a period of relatively high emissions (up to 2000 g m<sup>-2</sup> day<sup>-1</sup>). As described by Werner et al. (2014), fluxes were measured along fixed grid points using the accumulation chamber method (Rahn et al., 1996). In situ measurements were obtained using a West Systems® portable fluxmeter equipped with a LI-COR820 infrared gas analyzer. Based on statistical analysis, Werner et al. (2014) found soil CO<sub>2</sub> fluxes measured within areas of volcanic CO<sub>2</sub> emissions to be significantly elevated over background areas that were dominated by soil respiration of CO<sub>2</sub>. Maps of soil CO<sub>2</sub> flux were simulated from in-situ measurements at 1 m resolution using a sequential Gaussian simulation algorithm by these authors and we resampled their data to the Airborne Visible/Infrared Imaging Spectrometer (AVIRIS) resolution (13 m) using nearest neighbour resampling. Conventionally, studies of diffuse soil degassing of CO<sub>2</sub> on volcanoes have emphasized understanding of the modes, locations, geometries, and changes in volcanic flank degassing for purposes of volcanological research, hazard assessment, and monitoring. In many cases, volcanologists have focussed on areas associated with sufficient emissions of heat and CO<sub>2</sub> that vegetation has been killed off. In this study however, we focussed on vegetated areas where somewhat more mildly enhanced levels of volcanic CO<sub>2</sub> emissions into the forest ecosystems might be beneficial for plant growth, rather than adverse. As such, we



investigated zones and gradients *around* tree-kill areas, excluding areas that were barren or contained dead trees by filtering by fractional vegetation cover, where appropriate. In addition, because tree-kill areas on Mammoth Mountain are largely associated with “cold” CO<sub>2</sub> emissions, we completely avoided confounding influences of hydrothermal heat or acidic vapour emission on ecosystem response. The use of a high-spatial-resolution time-averaged (to limit the influence of varying meteorological conditions) map of canopy-level atmospheric CO<sub>2</sub> concentration would be most applicable to assess ecosystem response to elevated atmospheric CO<sub>2</sub> concentrations. However, such maps are unavailable. We therefore took advantage of the extensive record of soil CO<sub>2</sub> fluxes available for Mammoth Mountain. Although the effects of elevated CO<sub>2</sub> in the soil may be difficult to de-convolve from elevated CO<sub>2</sub> in the atmosphere, we treat their effects uniformly. Implications of this are discussed below.

Although the AVIRIS, MASTER, and ASO lidar datasets cover a wider region, only points with associated soil CO<sub>2</sub> flux measurements were used to derive our models. The CO<sub>2</sub> flux measurements were spatially resampled to match the resolution of the other datasets, which resulted in small estimations with low confidence along the edges. To avoid spurious model fits, edge points with CO<sub>2</sub> < 5 g m<sup>-2</sup> d<sup>-1</sup> were excluded, where the CO<sub>2</sub> range is [0,2000] g m<sup>-2</sup> d<sup>-1</sup>. In the remainder of this manuscript, analysed points with elevated CO<sub>2</sub> flux will be referred to as eCO<sub>2</sub>.

### 2.1.2 AVIRIS

The Airborne Visible/Infrared Imaging Spectrometer (AVIRIS) Classic instrument acquires data from 400 to 2500 nm in 224 contiguous spectral channels. AVIRIS imagery was acquired over Mammoth in October 2014; this flight was chosen from a number of possible surveys of the area to minimize snow cover, and also because of its temporal proximity to the eCO<sub>2</sub> ground measurements. The standard level 2 (L2) atmospherically corrected reflectance data (Thompson et al., 2015) was used (available from <https://aviris.jpl.nasa.gov/>), and the data had a spatial resolution of 13 m. This data was collected as part of the NASA HypSIRI Preparatory Airborne Campaign.

#### *Vegetation indices*

Vegetation indices are commonly used as an indicator of vegetation health and/or greenness. The following indices were derived from the AVIRIS spectral data:

- The Normalized Difference Vegetation Index (NDVI)
- Simple Ratio Index
- Enhanced Vegetation Index



- Red Edge Normalized Difference Vegetation Index
  - Modified Red Edge Simple Ratio Index
  - Modified Red Edge Normalized Difference Vegetation Index
  - Vogelmann Red Edge Index 1
- 5 Each uses a ratio between narrow bands to represent vegetation health as a single index, and all are described more fully in (Thenkabail et al., 2016).

#### *Foliar traits*

10 The chemical composition of plants affects light interactions, especially in the short-wave infrared (Singh et al., 2015). Therefore, imaging spectroscopy can be used to map key vegetation properties, especially those affecting carbon and nutrient interactions. Spectral features, derived from data such as AVIRIS, have been shown to correlate significantly with certain chemicals and plant properties, such as carbon, nitrogen, nitrogen isotope  $\delta^{15}\text{N}$ , Leaf Mass per Area (LMA), cellulose, and acid digestible lignin (Singh et al., 2015). These  
15 properties are associated with photosynthesis, light-harvesting ability, nutrient fluxes, and can be used to characterise vegetation responses to disturbances or climate trends (Townsend et al., 2008).

20 The data were first corrected for its bi-directional reflectance distribution function (BRDF), using the Ross-Thick BRDF model with a quadratic volumetric scattering term (Roujean et al., 1992; Lucht et al., 2000). In situ vegetation chemical measurements, along with propagated uncertainties, were used to derive partial least squares regression models for each trait. Since these equations were derived in the nearby area of the Sierra Nevada Mountains, these equations were applied to the BRDF-corrected AVIRIS data used in this study.

25 Infeasible negative numbers were removed for the modelling.

#### **2.1.3 MASTER**

The MODIS/ASTER (MASTER) airborne simulator acquires data in 50 channels between 0.4 – 13  $\mu\text{m}$ . We utilized the five thermal channels (10 – 13  $\mu\text{m}$ ), which had been processed  
30 to Level 2 (available from <https://master.jpl.nasa.gov/>). MASTER data were acquired in November 2013, with a 50 m spatial resolution.

#### *Land Surface Temperature*

35 The five thermal bands from MASTER were used to calculate Land Surface Temperature (LST) in a standard Level 2 product. The acquired data were processed to radiance using MODTRAN 5.2 for the atmospheric correction, along with a water vapour scaling method



(Tonooka, 2005). The Temperature Emissivity Separation (TES) algorithm was then used to derive LST and spectral emissivity (Gillespie et al., 1998).

5 The MASTER data are at coarser spatial resolution (50 m) compared to the other datasets (e.g., the working resolution for reprojection is the AVIRIS resolution of 13 m). An ideal dataset would have MASTER acquired at 13 m, or similar (~10 m; i.e., the scale of an individual tree canopy), but in order to build a comparable dataset for this analysis, we used two resampling methods: the standard nearest neighbour resampling; and a statistically principled method proposed in Ma et al. (2018). The statistical model proposed by Ma et al. 10 (2018) represented LST as a combination of low-dimensional random effects linked with basis functions and a Gaussian graphical model (also called Gaussian Markov random field). As demonstrated by the authors, this model provides a flexible and computationally efficient way to characterize potentially complex and nonstationary spatial variability. The parameters of the underlying statistical model were fitted to MASTER LST and ET data at 50 m 15 resolution, using maximum likelihood estimation via an Expectation-Maximization (EM) algorithm. The resampled data at 13 m spatial resolution were then generated via conditional statistical simulation in which we required that when aggregated back to the original coarse resolution, the resampled data matched the original MASTER data exactly.

#### 20 *Evapotranspiration*

Evapotranspiration (ET) is the key water variable in ecosystem functioning, indicating plant water use and loss (Fisher et al., 2017). In this study, ET was calculated using the PT-JPL retrieval (Fisher et al., 2008), which partitions ET into canopy transpiration, soil evaporation, and interception evaporation by transforming potential ET (Priestley and Taylor, 1972) into 25 actual ET using ecophysiological constraints. The ECOSTRESS ET retrieval system was used to incorporate MASTER LST as the thermal input (Fisher et al., 2015); additional ancillary data were incorporated from MODIS and Landsat to constrain meteorological and phenological controls on ET (Verma et al., 2016; Famiglietti et al., 2018; Ryu et al., 2011; Kobayashi et al., 2008). The final ET product used here was only the canopy transpiration 30 component (referred to as ET throughout), as our analytical interest lies only in the vegetation response to eCO<sub>2</sub>.

#### 2.1.4 ASO

35 The Airborne Snow Observatory (ASO, <http://aso.jpl.nasa.gov>) is a coupled lidar (Riegl Q1560) and spectrometer (CASI-1500) mounted on a King Air A90 aircraft, and was originally developed to monitor snow in the mountains for water resource management (Painter et al., 2016). The Riegl Q1560 is a dual scanning lidar with two 1064 nm laser sources; each scanner is tilted in the along-track direction by  $\pm 8^\circ$  and the cross-track direction



by  $\pm 14^\circ$  for enhanced retrieval of vertical surfaces. On June 27, 2017 ASO surveyed Mammoth Mountain, retrieving comprehensive lidar point cloud data at a mean of  $7.8 \text{ pt. m}^{-2}$  (max. value  $\sim 60 \text{ pt m}^{-2}$ ). Riegl RiPROCESS software was then used to a) extract point cloud data from raw waveforms (RiANALYZE) using the RiMTA Multiple Time Around  
5 algorithm and the RLMS Simple Classification Procedure for classification (SCP1), b) georeference the point cloud (RiWORLD), and c) export the point cloud to LAS 1.2 in UTM projection (RiWORLD).

#### *Digital Terrain Model*

10 The ASO lidar point cloud data were filtered to remove outliers by applying an elevation filter to eliminate points that exceed  $\pm 100 \text{ m}$  from a baseline digital terrain model (DTM) that was obtained from the USGS (United States Geological Survey). The ASO data processing chain includes the identification of ground and off-ground points using the Multiscale Curvature Classification algorithm (Evans and Hudak, 2007) and the calculation of a DTM (3  
15  $\text{m} \times 3 \text{ m}$ ) that corresponds to the bare soil surface as interpolated from the lidar points classified as ground. Any data voids were then in-filled using search windows that were centred on each void pixel.

#### *Slope and Aspect*

20 The slope (steepness) and aspect (direction) were derived directly from the DTM with the terrain analysis processing tool provided by QGIS. These geo-algorithms use a first-order derivative estimation to calculate the slope angle for each pixel in degrees relative to the horizontal plane and the slope exposition in degrees counter-clockwise from north. Aspect was processed to account for circular angles, by considering:

$$25 \quad K1 = \sin(\alpha + (90 - d)) + 1 \quad (1)$$

$$K2 = \cos(d - \alpha) + 1 \quad (2)$$

where  $\alpha$  is the aspect derived from the DTM as described above, and  $d$  is the prevailing wind direction. In the absence of local data, we assumed the prevailing wind direction to be  $270^\circ$  (e.g. Anderson and Farrar, 2001; Lewicki et al., 2008; Lewicki and Hilley, 2014). (Note, the  
30 results presented below were not sensitive to this assumption.)

#### *Canopy Height and Biomass*

The aboveground biomass (AGB) map ( $30 \text{ m} \times 30 \text{ m}$ ) was calculated by integrating ASO lidar measurements on forest structure and field inventory data into an allometric equation  
35 developed by Garcia et al., (2017):

$$AGB = 11.50 \times MCH^{1.20} \times FC^{0.88} \quad (3)$$



where MCH and FC are lidar-derived maps of mean canopy height and fractional cover, respectively. Eq. 3 was calibrated using AGB reference values derived from 69 field inventory plots located in the Stanislaus National Forest and Yosemite National Park, Sierra Nevada, California. To compute the lidar-derived maps, we first normalized the ASO lidar point cloud to calculate the effective height of vegetation by removing the effect of topography using the DTM described here above. Then, we used the normalized point cloud to calculate a canopy height model (CHM, 1m x 1m) by selecting the highest lidar point within each grid cell. Finally, the MCH was calculated by averaging the CHM within each 30 m cell, whereas the FCC was computed as the ratio of grid cells covered by vegetation (i.e. MCH>2 m) to the total number of cells. Note that we defined both MCH and FC with a grid cell size of 30 m in order to agree with the size of the field samples (Garcia et al., 2017). We assumed that Eq. 3 was transferable to our study site because the calibration plots are located only 80 km apart and they are both populated by vegetation of the upper montane and subalpine biotic zones.

15

### 2.1.5 Compiling the Dataset

The data were first processed to create derived products, and then geolocated to the AVIRIS native resolution of 13 m. That is, for each AVIRIS pixel, the other datasets were resampled and reprojected so that every pixel is associated with a vector of remotely sensed and derived values. Datasets with finer resolution (soil CO<sub>2</sub> flux and lidar) were averaged using the nearest neighbour principle. Derived products with coarser resolution (fractional cover, biomass, and evapotranspiration) were resampled using nearest neighbour resampling (e.g. the same biomass value may cover multiple AVIRIS pixels). Because its pixels were the largest, ET was also resampled using a statistically based method, described above in Section 2.1.3. We note that although the downscaling approach is robust and statistically sound, we acknowledge that our statistical estimates involving ET will include some uncertainty due to spatial resolution.

Once all pixels had been resampled, we had a total of 5520 data points. For certain experiments we found it necessary to threshold by fractional vegetation cover (FC>0.7; n=55), although the full dataset was used wherever possible.

The dates of acquisition also differed across datasets. The soil CO<sub>2</sub> flux datasets used in this study were measured during a peak in CO<sub>2</sub> emissions (Werner et al., 2014), which is thought to affect plant growth after the fact. However, we are observing a snap shot of vegetation function within a zone small enough to be influenced by the same meteorological inputs, and our models have accounted for confounding factors such as slope, elevation, and aspect.

35



Therefore, we considered measurements to be relative on a spatial scale, by comparing neighbouring pixels. The topographic confounders and the fractional cover are derived from the lidar data acquired four years after the MASTER data; however, we do not expect changes in the terrain during that time period, and tree presence is unlikely to have changed significantly.

## 2.2 Statistical Modelling

The variables assessed included: vegetation indices; plant foliar traits; evapotranspiration; canopy height; and, biomass. Given this combination of variables, we tested whether changes in eCO<sub>2</sub> were associated with significant changes in vegetation. We performed a series of multiple linear regressions using eCO<sub>2</sub> as a predictor of various vegetation variables; in particular, regression ensembles build collections of linear regression models, utilizing different predictor combinations, including multiplication of predictor variables. To control for confounding variables including elevation, slope, and aspect (which are topographic proxies for temperature, moisture, and light), we included them as predictors in the model. Then, the regression coefficient estimate for eCO<sub>2</sub> is an estimate of the change in the response variable due to a change in eCO<sub>2</sub>, holding all other variables in the model (the confounders) constant.

Fractional vegetation cover (FC; derived from the lidar) was considered a proxy for vegetation presence. The geometric variables elevation, slope, and aspect were also derived from the lidar point cloud, as described above. Figure 3 illustrates the stratified behaviour of NDVI as coloured by the four confounding variables. There is a particularly clear separation for fractional cover, which reinforces an expected result: eCO<sub>2</sub> had negligible effect on vegetation indices and other variables over bare ground, but showed higher impacts on fully vegetated pixels. Therefore, we model each vegetation variable,  $V$ , as

$$V = b_1 C + b_2 F + b_3 S + b_4 A + b_5 E + f(C, F, S, A, E) + \varepsilon \quad (4)$$

where  $C$  is the elevated soil CO<sub>2</sub> flux,  $F$  is the fractional vegetation cover,  $S$  is the slope,  $A$  is the aspect,  $E$  is the elevation, and  $\varepsilon \sim N(0, \sigma^2)$  is random error. The function  $f(\cdot)$  describes relationships between the predictor variables, which for this model is limited to the first order interactions:

$$f(C, F, S, A, E) = b_6 C \cdot F + b_7 C \cdot S + b_8 C \cdot A + b_9 C \cdot E + b_{10} F \cdot S + \dots \quad (5)$$

Our hypothesis is  $H_A: b_1 \neq 0$ , that is, that the effect of eCO<sub>2</sub> on vegetation variable  $V$



is different from zero. Our null hypothesis is then  $H_0, b_1 = 0$ .

Certain other confounding variables may affect the modelled relationships. The following scenarios and/or variables were also tested as confounders, but did not affect the model

- 5 outcome: pixel position; site number; and species (plant species were estimated by performing an unsupervised classification on the AVIRIS data). The eCO<sub>2</sub> dataset was also shifted to simulate winds and atmospheric pressure (Ogretim et al., 2013). This did not have an impact on the results.
- 10 When evaluating the dynamics between different variables, it is assumed that the study from which our ground measurements were derived (Werner et al., 2014), covered most of the known CO<sub>2</sub> diffuse emission areas, and so the remainder of the scene exists as a control. The control pixels were also thresholded according to the range of the confounding variables found for the eCO<sub>2</sub> points. Therefore, we considered only control points with elevation,
- 15 slope, and aspect values, respectively, between 2700 and 2950 m, less than 350°, and less than 30°.

### 3 Statistical Estimation

Although the models were run for 42 explanatory variables (including additional vegetation indices, foliar traits, and other vegetation descriptors), for the sake of brevity we only present

- 20 the best performing variables (traits with significant p-values are shown, and for all other variables, those with significant p-values and  $R^2 > 0.5$ ). For the variables shown in Table 2, the p-value of the eCO<sub>2</sub> term,  $b_1$ , was for each model  $< 0.05$ , and in most cases  $\ll 0.05$ . The most significant predictor was determined by ordering terms by p-values.

- 25 As the confounding variables are expected to drive the behaviour of ecosystem properties, a reduced eCO<sub>2</sub> “rank” (in terms of p-value significance) does not negate the impact of eCO<sub>2</sub> in the models; in fact, each ecosystem variable was strongly influenced by increasing eCO<sub>2</sub>, given the low p-values for the eCO<sub>2</sub> coefficient in each model.



## 4 Results

### 4.1 Structure: Canopy Height and Biomass

Canopy height and biomass were well modelled, as seen in Table 2 and Figure 4, although  $eCO_2$  was the least significant predictor. In each case,  $eCO_2$  was still regarded as statistically significant, but had lower predictive power than the topographic variables.

Figure 5 shows the predictor variable  $eCO_2$  against the predicted biomass. There is variability at low  $eCO_2$  levels, but overall a small decrease in biomass with increasing  $eCO_2$ . This decrease appears to saturate, and is better fit by a logarithmic function, however, given that interactions between terms in the model is allowed, we do not necessarily expect a linear fit, since the  $eCO_2$  contribution to the model may be multiplied by other confounding variables.

### 4.2 Composition: Vegetation Indices and Foliar traits

The performance of different vegetation indices and foliar traits varied. NDVI was best modelled, with an  $R^2$  of 0.68, and with  $eCO_2$  as the most significant predictor (p-value of  $1e-12$ ). In general, the indices were better modelled than the traits.

Figure 6 shows the predicted model for NDVI (a) and the canopy nitrogen concentration trait (b) against the  $eCO_2$  predictor variable. Modelled NDVI decreases with increasing  $eCO_2$ , and there is a decrease in variance with increasing  $eCO_2$ . The modelled canopy nitrogen concentration trait increases with increasing  $eCO_2$ .

### 4.3 Function: Evapotranspiration

Canopy transpiration was relatively well represented by the  $eCO_2$  model with an  $R^2 = 0.55$ . For comparison, total ET was not well represented by the  $eCO_2$  model ( $R^2 = 0.23$ ), which is sensible, as  $eCO_2$  is expected to affect only plant transpiration and not soil evaporation.  $eCO_2$  was the second most significant predictor, with fractional vegetation cover the most significant. Given that MASTER data were originally acquired at a much coarser resolution (50 m) than the  $eCO_2$  ground data (1 m), and that both were resampled to 13 m resolution for the overall consistent analysis, there may have been error introduced due to the resampling. This effect is seen by the much lower model fit with the statistical resampling, although the predicted models follow the same trend. In the remainder of the manuscript, references to ET refer to the data resampled using nearest neighbour resampling.

Figure 7 shows the ET predicted by the model for the predictor variable  $eCO_2$ . There is a decrease in ET for increasing  $eCO_2$ , along with a decrease in variance.



#### 4.4 Ecosystem synergies

Given that many of the vegetation indices and traits are only appropriate in the presence of vegetation, a fractional cover threshold of 0.7 was used for the eCO<sub>2</sub> sample, for the sake of evaluating the dynamics between modelled variables. With this threshold, only 55 data points remained, and so the sample size is too small to make claims of statistical significance. Therefore, we present the following results as interesting observations that may inform future data acquisition.

Figure 8 shows the dynamics between variables in the entire scene (i.e., non-elevated, background soil CO<sub>2</sub>) versus the points with eCO<sub>2</sub> measurements. It is important to note that in each sub-figure, independent data sources are used to avoid showing intrinsically correlated datasets. Fractional cover and biomass are derived from the ASO lidar data; the vegetation trait data and foliar traits are derived from AVIRIS imagery; and ET is derived from MASTER data. In this case, the variables shown are directly as observed (or derived directly from the data source).

We observed interesting dynamics between ecosystem variables, suggesting great potential for future research. In the eCO<sub>2</sub> subset, NDVI was, on average, lower than that observed for the same fractional cover in the control dataset (Figure 8 a). This is consistent with the model illustration of decreased greenness for increasing eCO<sub>2</sub>. Similarly, ET was lower in the eCO<sub>2</sub> subset for pixels with the same NDVI observed in the control, showing a greater degree of stress even when plants have the same greenness (Figure 8 b). In addition, the strong linear relationship between ET and NDVI appears to break down for the points affected by eCO<sub>2</sub>.

Canopy nitrogen in the eCO<sub>2</sub> subset increased with fractional cover, unlike the control which remained flat, which again mimics the modelled data findings (Figure 8 c). ET was lower in the eCO<sub>2</sub> subset for the same biomass, which implies that plants are doubly affected by the enhanced CO<sub>2</sub> – the biomass decreases with increasing eCO<sub>2</sub>, and the ET decreases further with decreasing biomass (Figure 8 d). Again, the strong linear relationship between ET and biomass breaks down for those points affected by eCO<sub>2</sub>. These findings suggest complex relationships between ecosystem parameters in their response to increasing eCO<sub>2</sub>.

#### 5. Discussion

Using airborne remotely sensed ecosystem properties against a ground measured database of eCO<sub>2</sub> (volcanic excess CO<sub>2</sub> emanating into the forest canopy through the soil), we evaluated the effects of increasing eCO<sub>2</sub> on plant structure, function, and composition. Our aims were



to: (i) evaluate whether a passively degassing volcanic system is a viable means to study properties of ecosystems; (ii) determine if ecosystem variables are adequately detected using airborne data; and (iii) present key lessons learnt that can enable similar studies over different biomes.

5

This study has provided initial observations of ecological responses to eCO<sub>2</sub> that are measurable from airborne data. We found that a) eCO<sub>2</sub> was a significant predictor in regression ensemble models of ecosystem variables, and b) there were visual differences between the sites of increased eCO<sub>2</sub> and the background image. This work also demonstrates that an active volcanic system is a viable way in which to study the CO<sub>2</sub> effect on ecosystems.

10

The regression ensemble model showed that eCO<sub>2</sub> was a significant predictor for two structural variables (canopy height and biomass), nine composition variables (6 vegetation indices, 3 foliar traits), and a function variable (ET). Therefore, as hypothesised, eCO<sub>2</sub> affects ecosystems in structure, composition, and function, all of which are detectable both with airborne observations as well as within a volcanically-derived eCO<sub>2</sub> system. Further evaluation of the model showed that both canopy height and biomass decreased with increasing eCO<sub>2</sub>; the vegetation indices decrease with increasing eCO<sub>2</sub>; canopy nitrogen concentration increases; LMA decreases; Carbon decreases; and ET decreases.

15

20

Some of these observations contrasted with results found in other published studies, while others agreed. For instance, our study found a decrease in NDVI with increasing eCO<sub>2</sub>, which correlates to the multispectral satellite findings of Rouse et al. (2010) and Cholathat et al., (2011). In some cases, the decrease can be explained by the tree-kill effect, where vegetation is removed. However, by accounting for fractional cover in our models, we have shown that NDVI decreases independently from fractional cover (see in Figure 8). This shows that, regardless of whether the number of trees changes, the greenness of individual trees is reduced. This finding is in direct contrast with the CO<sub>2</sub> fertilization hypothesis which states that rising CO<sub>2</sub> has a positive effect on plant growth and productivity due to increased availability of carbon, and which has been shown using field data (Huang et al., 2007; Zhu et al., 2016). The decrease in canopy height and biomass agrees with the tree-ring study done by Biondi and Fessenden (1999), which also found slower Lodgepole Pine growth rates in high CO<sub>2</sub> emission areas on Mammoth Mountain. However, a study by Smith et al. (2013) found an increase in biomass in the mixed-species temperate forest FACE experiment. In that experiment, there was large variation between and within species, and the experiment was limited to four years. Perhaps a long-term species composition shift due to eCO<sub>2</sub> was the

25

30

35



cause of the change in biomass in our study, but we do not have individual tree species-level data to support this hypothesis.

- Our model showed an increase in canopy nitrogen, which could indicate species selection or individual plant optimization, given the decrease in NDVI, biomass, and ET. Canopy nitrogen is associated with plant's investment in photosynthesis (Singh et al., 2015). We also found an increase in canopy nitrogen relative to fractional cover, showing that the change in nitrogen was not impacted by an increase in overall vegetation for those sites (Figure 8). Tercek et al. (2008) noted that *Dichanthelium lanuginosum* (hot springs panic grass) in Yellowstone had made physiological adjustments to photosynthetic enzymes in response to long-term exposure to CO<sub>2</sub>, and a study of ice cores showed a 40% decrease in stomatal density over the last 200 years, which paralleled an increase in global CO<sub>2</sub> (Woodward, 1987). However, Sharma and Williams (2009) evaluated vegetation naturally exposed to CO<sub>2</sub> in Yellowstone National Park, and found reduced nitrogen at a leaf level in *Pinus contortus* (Lodgepole Pine), and increased nitrogen at a leaf level for *Linaria dalmatica* (Dalmation Toadflax; an invasive, non-native herb). Once again, the species-level differences highlight the need for remote sensing analysis over areas that encompass wide species variation, in order to understand overall trends.
- Kimball et al. (1998) found a slight increase in ET in a FACE experiment over cotton fields, but that increase was within the error of the ET estimation, and so was not deemed statistically significant. In contrast, Nendel et al. (2009) found a decrease in ET, and an increase in dry above-ground biomass over a FACE crop rotation experiment. In this study, we found a decrease in ET. In addition, we found a decrease in ET relative to both NDVI and biomass, when comparing the points affected by eCO<sub>2</sub> to those unaffected points in the surrounding area. The unaffected sites showed a positive linear relationship between ET and both NDVI and biomass, which appeared to break down for points affected by eCO<sub>2</sub> in both relationships.
- High fluxes of CO<sub>2</sub> through soils on Mammoth Mountain have likely impacted forest ecosystems through oxygen deprivation in soil pore space, inhibition of root respiration and soil acidification (Farrar et al., 1995; Qi et al., 1994; McGee and Gerlach, 1998). Since we used soil CO<sub>2</sub> flux as the predictor variable in the model, some of the observed ecosystem responses may therefore be due to the effects of high concentrations of CO<sub>2</sub> on the soil environment or some combination of soil and atmospheric effects. The Mammoth Mountain soil CO<sub>2</sub> flux dataset does, however, provide a record of CO<sub>2</sub> emissions that is more stable in space and time than measurements of atmospheric CO<sub>2</sub> concentrations. In particular, forest canopies will through time be exposed to eCO<sub>2</sub> at highly variable levels, because eCO<sub>2</sub> once



emitted through the soil into the sub-canopy atmosphere is subject to highly variable dispersion from thermal and wind disturbances at minutes, diurnal, and seasonal scales (Staebler and Fitzjarrald, 2004). In-canopy concentration measurements of eCO<sub>2</sub> will therefore be highly variable, and especially if conducted instantaneously, may not be  
5 representative of the long-term relative exposure strength in the canopy.

This exploratory study leveraged existing data acquired over Mammoth Mountain. We used ASO lidar, AVIRIS, and MASTER data to derive products that describe ecosystem structure, composition, and function, and used field eCO<sub>2</sub> measurements to show that elevated CO<sub>2</sub> was  
10 a significant predictor of ecosystem variables, including vegetation indices, plant foliar traits, biomass, and evapotranspiration. While our study has shown the promise of airborne remote sensing in detecting measurable ecosystem changes in forest ecosystems on and around a CO<sub>2</sub>-emitting volcanic system, it was also completed using an existing ad-hoc collection of data. The nature of the collection of data sources enabled us to understand the details of the  
15 data characteristics necessary for future studies.

While this study is useful for showing the benefit of both a passively emitting volcanic system and airborne data for evaluating the ecosystem response to eCO<sub>2</sub>, we anticipate that more meaningful results would be obtained with all datasets acquired simultaneously, at the  
20 same resolution. ET in particular varies over short time periods due to the influence of meteorological inputs, and so multi-temporal acquisitions would provide a better overview of the ecosystem function. Other data, such as photosynthesis, may also add to future analysis.

## 6. Conclusions

This exploratory study used airborne remote sensing data, coupled with ground  
25 measurements of soil CO<sub>2</sub> flux on a forested volcano, to derive relationships between rising CO<sub>2</sub> emissions and ecosystem structure, function, and composition metrics. We have shown that passively emitting volcanic systems are viable environments in which to study CO<sub>2</sub> impacts on ecosystems, with eCO<sub>2</sub> the most significant predictor in regression ensemble models of several ecological variables, including NDVI, canopy nitrogen concentration, ET,  
30 and biomass. When comparing differences between vegetation parameters affected by eCO<sub>2</sub> and those estimated over the background scene, we found contrasting patterns and dynamics between ecological variables, showing that a combination of different remote sensing platforms is capable of providing a comprehensive view of ecosystem responses to volcanic CO<sub>2</sub>.  
35

Key lessons learnt from this study include:



1. Future campaigns should acquire all data at the same or similar resolution, at individual tree-scale
2. More than 55 vegetated tree points are necessary in order to draw meaningful conclusions regarding the dynamics between variables
- 5 3. Combining lidar and spectral data across a range of wavelengths yielded a more complete view than using any one data source alone.

## 6. Acknowledgements

We thank Cynthia Werner for providing soil CO<sub>2</sub> flux data over our study area; Gregory Halverson for processing ET data; Zhiwei Ye for processing functional trait data; and  
10 Anthony Bloom, Stuart Wilkinson, Christoph Kern, and Deborah Bergfeld for discussions during earlier stages of this project. The research described in this paper was carried out at the Jet Propulsion Laboratory, California Institute of Technology, under contract with the National Aeronautics and Space Administration. © 2018 California Institute of Technology. Government sponsorship acknowledged.

## 15 References

- Anderson, D. E., and Farrar, C. D.: Eddy covariance measurement of CO<sub>2</sub> flux to the atmosphere from an area of high volcanogenic emissions, Mammoth Mountain, California. *Chem. Geol.*, 177, 31–42, 2001.
- 20 Biondi, F. and Fessenden, J. E.: Response of Lodgepole Pine growth to CO<sub>2</sub> degassing at Mammoth Mountain, California. *Ecology*, 80(7), 2420–2426, 1999.
- Boudoire, G., Di Muro, A., Liuzzo, M., Ferrazzini, V., Peltier, A., Gurrieri, S., Michon, L., Giudice, G., Kowalski, P. and Boissier, P.: New perspectives on volcano monitoring in a tropical environment: Continuous measurements of soil CO<sub>2</sub> flux at Piton de la Fournaise (La Réunion Island, France). *Geophys. Res. Lett.*, 44, 8244–8253, 2017.
- 25 Camarda, M., De Gregorio, S. and Gurrieri, S.: Magma-ascent processes during 2005–2009 at Mt Etna inferred by soil CO<sub>2</sub> emissions in peripheral areas of the volcano. *Chem. Geol.*, 330, 218–227, 2012.
- Cardellini, C., Chiodini, G., Frondini, F.: Application of stochastic simulation to CO<sub>2</sub> flux from soil: mapping and quantification of gas release. *J. Geophys. Res.*, 108, 2425,  
30 2013.
- Cholathat, R., Li, X., Ge, L.: Monitoring natural analog of geologic carbon sequestration using multi-temporal Landsat TM images in Mammoth Mountain, Long Valley Cadera, California. *Int. Geosci. Remote Se.*, Vancouver, 24–29 July 2011, 2011.



- Cook, A. C., Hainsworth, L. J., Sorey, M. L., Evans, W. C., Southon, J. R.: Radiocarbon studies of plant leaves and tree rings from Mammoth Mountain, CA: a long-term record of magmatic CO<sub>2</sub> release. *Chem. Geol.*, 177, 117-131, 2001.
- 5 Drake, B. G., González-Meler, M. A., and Long, S. P.: More Efficient Plants: A Consequence of Rising Atmospheric CO<sub>2</sub>? *Annu. Rev. Plant Phys.*, 48(1), 609–639. doi: 10.1146/annurev.arplant.48.1.609, 1997.
- Evans, J. S., Hudak, A. T.: A multiscale curvature algorithm for classifying discrete return LiDAR in forested environments. *IEEE T. Geosci. Remote*, 45, 1029–1038. doi:<http://dx.doi.org/10.1109/TGRS.2006.890412>, 2007.
- 10 Farrar, C. D., Sorey, M. L., Evans, W. C., Howle, J. F., Kerr, B. D., Kennedy, B. M., ... Southon, J. R.: Forest-killing diffuse CO<sub>2</sub> emission at Mammoth Mountain as a sign of magmatic unrest. *Nature*, 376(6542), 675–678. Retrieved from <http://dx.doi.org/10.1038/376675a0>, 1995.
- 15 Fisher, J. B., and ECOSTRESS Algorithm Development Team.: ECOSystem Spaceborne Thermal Radiometer Experiment on Space Station (ECOSTRESS): Level-3 Evapotranspiration Algorithm Theoretical Basis Document, 24 pp, Jet Propulsion Laboratory, Pasadena, 2015.
- Fisher, J. B., Melton, F., Middleton, E., Hain, C., Anderson, M., Allen, R., McCabe, M. F., Hook, Baldocchi, D., Townsend, P. A., Kilic, A., Tu, K., Miralles, D. D., Perret, J., Lagouarde, J.-P., Waliser, D., Purdy, A. J., French, A., Schimel, D., Famiglietti, J. S., Stephens, G., Wood, E. F.: The Future of Evapotranspiration: Global requirements for ecosystem functioning, carbon and climate feedbacks, agricultural management, and water resources. *Water Resour. Res.*, 53(4), 2618-2626, 2017.
- 20 Fisher, J. B., Tu, K., Baldocchi, D. D.: Global estimates of the land-atmosphere water flux based on monthly AVHRR and ISLSCP-II data, validated at 16 FLUXNET sites. *Remote Sens. Environ.*, 112, 901-919, 2008.
- Friedlingstein, P., Meinshausen, M., Arora, V. K., Jones, C. D., Anav, A., Liddicoat, S. K., Knutti, R.: Uncertainties in CMIP5 Climate Projections due to Carbon Cycle Feedbacks. *J. Climate*, 27, 512-526, 2014.
- 30 Garcia, M., Saatchi, S., Ferraz, A., Silva, C.A., Ustin, S., Koltunov, A., Balzter, H.: Impact of data model and point density on aboveground forest biomass estimation from airborne LiDAR. *Carbon Balance and Management*, 12. doi:10.1186/s13021-017-0073-1, 2017.
- Gerlach, T. M.: Present-day CO<sub>2</sub> emissions from volcanos. *Eos Trans AGU*, 72(23), 249–255. doi: 10.1029/90EO10192, 1991.
- 35 Giammanco, S., Sims, K. W. W., and Neri, M.: Measurements of <sup>220</sup>Rn and <sup>222</sup>Rn and CO<sub>2</sub> emissions in soil and fumarole gases on Mt. Etna volcano (Italy): Implications for gas



- transport and shallow ground fracture. *Geochem. Geophys. Geosy.*, 8(10)  
<https://doi.org/10.1029/2007GC001644>, 2007.
- 5 Gillespie, A., Rokugawa, S., Matsunaga, T., Cothorn, J.S., Hook, S.J., and Kahle, A.B.: A temperature and emissivity separation algorithm for Advanced Spaceborne Thermal Emission and Reflection Radiometer (ASTER) images. *IEEE T. Geosci. Remote Sens.*, 36, 1113–1126, 1998.
- Hernández, P. A., Pérez, N. M., Salazar, J. M., Nakai, S., Notsu, K., and Wakita, H.: Diffuse emission of carbon dioxide, methane, and helium-3 from Teide Volcano, Tenerife, Canary Islands. *Geophys. Res. Lett.*, 25(17), 3311–3314.  
10 <https://doi.org/10.1029/98GL02561>, 1998.
- Huang, J.-G., Bergeron, Y., Denneker, B., Berninger, F., and Tardif, J.: Response of forest trees to increased atmospheric CO<sub>2</sub>, *Crit. Rev. Plant Sci.*, 26, 265–283, doi:10.1080/07352680701626978, 2007.
- Kerrick, D. M.: Present and past nonanthropogenic CO<sub>2</sub> degassing from the solid earth. *Rev. Geophys.*, 39(4), 565–585. <https://doi.org/10.1029/2001RG000105>, 2001.  
15
- Kimball, B. A., LaMorte, R. L., Seay, R. S., Pinter, P. J. Jr, Rokey, R. R., Hunsaker, D. J., Dugas, W. A., Heuer, M. L., Mauney, J. R., Hendrey, G. R., Lewin, K. F., Nagy, J.: Effects of free-air CO<sub>2</sub> enrichment on energy balance and evapotranspiration of cotton. *Agr. Forest Meteorol.*, 70, 259–278, 1998.
- 20 Kobayashi, H., and Iwabuchi, H.: A coupled 1-D atmosphere and 3-D canopy radiative transfer model for canopy reflectance, light environment, and photosynthesis simulation in a heterogeneous landscape, *Remote Sens. Environ.*, 112(1), 173–185, 2008.
- Kolby Smith, W., Reed, S. C., Cleveland, C. C., Ballantyne, A. P., Anderegg, W. R. L., Wieder, W. R., ... Running, S. W.: Large divergence of satellite and Earth system model estimates of global terrestrial CO<sub>2</sub> fertilization. *Nat. Clim. Change*, 6, 306. Retrieved from <http://dx.doi.org/10.1038/nclimate2879>, 2015.  
25
- Körner, C.: Plant CO<sub>2</sub> responses: an issue of definition, time and resource supply. *New Phytol.*, 172(3), 393–411. doi: 10.1111/j.1469-8137.2006.01886.x, 2006.
- 30 Le Quéré, C., Andrew, R. M., Canadell, J. G., Sitch, S., Korsbakken, J. I., Peters, G. P., ... Zaehle, S.: Global Carbon Budget 2016. *Earth Syst. Sci. Data*, 8(2), 605–649. doi: 10.5194/essd-8-605-2016, 2016.
- Lewicki, J. L. and Hilley, G. E.: Multi-scale observations of the variability of magmatic CO<sub>2</sub> emissions, Mammoth Mountain, CA, USA. *J. Volcanol. Geoth. Res.*, 284, 1–15, doi:10.1016/j.jvolgeores.2014.07.011, 2014.  
35
- Lewicki, J. L., Fischer, M. L., and Hilley, G. E.: Six-week time series of eddy covariance CO<sub>2</sub> flux at Mammoth Mountain, California: performance evaluation and role of



- meteorological forcing, *J. Volcanol. Geoth. Res.*, 171, 178-190, doi:10.1016/j.jvolgeores.2007.11.029, 2008.
- 5 Lewicki, J. L., Hilley, G. E., Shelly, D. R., King, J. C., McGeehin, J. P., Mangan, M.: Crustal migration of CO<sub>2</sub>-rich magmatic fluids recorded by tree-ring radiocarbon and seismicity at Mammoth Mountain, CA, USA. *Earth Planet. Sci. Lett.*, 390, 52-58, 2014.
- Lewin, K. F., Hendrey, G. R., Nagy, J., and LaMorte, R. L.: Design and application of a free-air carbon dioxide enrichment facility. *Agric. Forest Meteorol.*, 70(1), 15–29. [https://doi.org/https://doi.org/10.1016/0168-1923\(94\)90045-0](https://doi.org/https://doi.org/10.1016/0168-1923(94)90045-0), 1994.
- 10 List, M.R.: Geologic remote sensing and GIS evaluation of volcanogenic CO<sub>2</sub>-induced tree kills: Mammoth Mountain, California, 1991-2004, M.S. Thesis, CSUS, 2005.
- Ma, P., Kang, E. L., Braverman, A., and Nguyen, H.: Spatial statistical downscaling for constructing high-resolution nature runs in global observing system simulation experiments. In review. 2018.
- 15 Mason, E., Edmonds, M. and Turchyn, A. V.: Remobilization of crustal carbon may dominate volcanic arc emissions. *Science*, 357(6348), 290-294, 2017.
- McGee, K. A., and Gerlach, T. M.: Annual cycle of magmatic CO<sub>2</sub> in a tree-kill soil at Mammoth Mountain, California: Implications for soil acidification. *Geology*, 26(5), 463–466. Retrieved from [http://dx.doi.org/10.1130/0091-7613\(1998\)026%3C0463:ACOMCI%3E2.3.CO](http://dx.doi.org/10.1130/0091-7613(1998)026%3C0463:ACOMCI%3E2.3.CO), 1998.
- 20 McGuire, A. D., Melillo, J. M., and Joyce, L. A.: The Role of Nitrogen in the Response of Forest Net Primary Production to Elevated Atmospheric Carbon Dioxide. *Annu. Rev. Ecol. Syst.*, 26, 473–503. Retrieved from [http://harvardforest.fas.harvard.edu/sites/harvardforest.fas.harvard.edu/files/publications/pdfs/McGuire\\_AnReviewEcoandSys\\_1995.pdf](http://harvardforest.fas.harvard.edu/sites/harvardforest.fas.harvard.edu/files/publications/pdfs/McGuire_AnReviewEcoandSys_1995.pdf), 1995.
- 25 Nendel, C., Kersebaum, K. C., Mirschel, W., Manderscheid, R., Weigel, H.-J., Wenkel, K.-O.: Testing different CO<sub>2</sub> response algorithms against a FACE crop rotation experiment. *NJAS - Wageningen J. Life Sci.*, 57(1), 17-25, 2009.
- Norby, R. J., De Kauwe, M. G., Domingues, T. F., Duursma, R. A., Ellsworth, D. S., Goll, D. S., ... Zaehle, S.: Model–data synthesis for the next generation of forest free-air CO<sub>2</sub> enrichment (FACE) experiments. *New Phytol.*, 209(1), 17–28. doi: 10.1111/nph.13593, 2016.
- 30 Ogretim, E., Crandall, D., Gray, D. D., Bromhai, G. S.: Effects of Atmospheric Dynamics on CO<sub>2</sub> Seepage at Mammoth Mountain, California USA. *Journal of Computational Multiphase Flows*, 5(4), 283-294, 2013.
- 35 Painter, T. H., Berisford, D. F., Boardman, J. W., Bormann, K. J., Deems, J. S., Gehrke, F., Hedrick, A., Joyce, M., Laidlaw, R., Marks, D., Mattmann, C., McGurk, B., Ramirez, P., Richardson, M., Skiles, S. M., Seidel, F. C., Winstral, A.: The Airborne Snow



- Observatory: Fusion of scanning lidar, imaging spectrometer, and physically-based modeling for mapping snow water equivalent and snow albedo. *Remote Sens. Environ.*, 184, 139–152. <https://doi.org/10.1016/j.rse.2016.06.018>, 2016.
- 5 Perez, N. M., Hernandez, P. A., Padilla, G., Nolasco, D., Barrancos, J., Melian, G., ... Ibarra, M.: Global CO<sub>2</sub> emission from volcanic lakes. *Geology*, 39, 235–238, 2011.
- Peterson, B. J., and Melillo, J. M.: The potential storage of carbon caused by eutrophication of the biosphere. *Tellus B*, 37B(3), 117–127. doi: 10.1111/j.1600-0889.1985.tb00060.x, 1985.
- 10 Pickles, W. L., Kasameyer, P. W., Martini, B. A., Potts, D. C., Silver, E. A.: Geobotanical Remote Sensing for Geothermal Exploration. Geothermal Resources Council 2001 Annual Meeting, San Diego, California, August 26-29, 2001.
- Potter, D. A.: Forested Communities of the Upper Montane in the Central and Southern Sierra Nevada. United States Department of Agriculture General Technical Report PSW-GTR-169, 1998.
- 15 Qi, J., Marshall, J. D., and Mattson, K. G.: High soil carbon dioxide concentrations inhibit root respiration of Douglas fir. *New Phytol.*, 128, 435–442, 1994.
- Rahn, T. A., Fessenden, J. E., and Wahlen, M.: Flux chamber measurements of anomalous CO<sub>2</sub> emission from the flanks of Mammoth Mountain, California. *Geophys. Res. Lett.*, 23(14), pp.1861-1864, 1996.
- 20 RiANALYZE. Available online at <http://www.riegl.com/products/software-packages/rianalyze/> (accessed: 08/07/2017), 2017.
- Rouse, J. H., Shaw, J. A., Lawrence, R. L., Lewicki, J. L., Dobeck, L. M., Repasky, K. S., Spangler, L. H.: Multi-spectral imaging of vegetation for detecting CO<sub>2</sub> leaking from underground. *Environ. Earth Sci.*, 60, 313-323, 2010.
- 25 Ryu, Y., Baldocchi, D. D., Kobayashi, H., van Ingen, C., Li, J., Black, T. A., Beringer, J., van Gorsel, E., Knohl, A., Law, B. E. and Rouspard, O.: Integration of MODIS land and atmosphere products with a coupled-process model to estimate gross primary productivity and evapotranspiration from 1 km to global scales, *Global Biogeochem. Cycles*, 25(4), GB4017, 2011.
- 30 Schimel, D. S.: Terrestrial ecosystems and the carbon cycle. *Glob. Change Biol.*, 1(1), 77–91. doi: 10.1111/j.1365-2486.1995.tb00008.x, 1995.
- Schimel, D., Stephens, B. B., and Fisher, J. B.: Effect of increasing CO<sub>2</sub> on the terrestrial carbon cycle. *Proceedings of the National Academy of Sciences*, 112(2), 436–441. <https://doi.org/10.1073/pnas.1407302112>, 2015.
- 35 Schwandner, F. M., Gunson, M. R., Miller, C. E., Carn, S. A., Eldering, A., Krings, T., ... Podolske, J. R.: Spaceborne detection of localized carbon dioxide sources. *Science*, 358(6360). <http://dx.doi.org/10.1126/science.aam5782>, 2017.



- Schwandner, F. M., Seward, T. M., Gize, A. P., Hall, P. A. and Dietrich, V. J.: Diffuse emission of organic trace gases from the flank and crater of a quiescent active volcano (Vulcano, Aeolian Islands, Italy). *J. Geophys. Res. Atmospheres*, 109 (D4), D04301. DOI: 10.1029/2003JD003890, 2004.
- 5 Sharma, S. and Williams, D.G.: Carbon and oxygen isotope analysis of leaf biomass reveals contrasting photosynthetic responses to elevated CO<sub>2</sub> near geologic vents in Yellowstone National Park. *Biogeosciences*, 6, 25-31, 2009.
- Smith, A.R., Lukac, M., Hood, R., Healey, J. R., Miglietta, F., Godbold, D. L.: Elevated CO<sub>2</sub> enrichment induces a differential biomass response in a mixed species temperate forest plantation. *New Phytol.*, 198, 156-168, 2013.
- 10 Staebler, R. M., Fitzjarrald, D. R.: Observing subcanopy CO<sub>2</sub> advection. *Agr. Forest Meteorol.* 112 (3-4), 139-156, 2004.
- Tercek, M. T., Al-Niemi, T. S., Stout, R. G.: High Levels of Carbon Dioxide in Yellowstone National Park: A Glimpse into the Future? *Yellowstone Science*, 16(1), 12-19, 2008.
- 15 Thenkabail, P. S., Lyon, J. G. Huete, A.: *Hyperspectral Remote Sensing of Vegetation*. CRC Press, Taylor and Francis Group, 405 - 406, 2016.
- Thompson, D. R., Gao, B.-C., Green, R. O., Roberts, D. A., Dennison, P. E., Lundeen, S. R.: Atmospheric correction for global mapping spectroscopy: ATREM advances for the HypIRI preparatory campaign. *Remote Sens. Environ.*, 167, 64-77, 2015.
- 20 Tonooka, H.: Accurate Atmospheric Correction of ASTER Thermal Infrared Imagery Using the WVS Method, *IEEE Trans. Geos. Remote Sens.*, 43 (12), 2005.
- Verma, M., Fisher, J. B., Mallick, K., Ryu, Y., Kobayashi, H., Guillaume, A., Moore, G., Ramakrishnan, L., Hendrix, V., Wolf, S., Sikka, M., Kiely, G., Wohlfahrt, G., Gielen, B., Roupsard, O., Toscano, P., Arain, M. A., and Cescatti, A.: Global surface net-radiation at 5 km from MODIS Terra, *Remote Sensing*, 8(739), 1-20, 2016.
- 25 Werner, C. and Brantley, S.: CO<sub>2</sub> emissions from the Yellowstone volcanic system. *Geochem., Geophys., Geosy.*, 4(7), 1061, 2003.
- Werner, C., Bergfeld, D., Farrar, C. D., Doukas, M. P., Kelly, P. J., and Kern, C.: Decadal-scale variability of diffuse CO<sub>2</sub> emissions and seismicity revealed from long-term monitoring (1995–2013) at Mammoth Mountain, California, USA. *J. Volcanol. Geotherm. Res.*, 289 (Supplement C), 51–63. <https://doi.org/https://doi.org/10.1016/j.jvolgeores.2014.10.020>, 2014.
- 30 Woodward, F. I.: Stomatal numbers are sensitive to increases in CO<sub>2</sub> from pre-industrial levels, *Nature*, 327, 617-618., 1987.
- 35 Zhu, Z., Piao, S., Myneni, R. B., Huang, M., Zeng, Z., Canadell, J. G., Ciais, P., Sitch, P., Friedlingstein, P., Arneeth, A., Cao, C., Cheng, L., Kato, E., Koven, C., Li, Y., Lian, X., Liu, Y., Liu, R., Mao, J., Pan, Y., Peng, S., Peñuelas, J., Poulter, B., Pugh, T. A. M., Stocker, B. D., Viogy, N., Wang, X., Wang, Y., Xiao, Z., Yang, H., Zaehle, S.



and Zeng, N.: Greening of the Earth and its drivers, *Nat. Clim. Change*, 6, 791-795, 2016. a

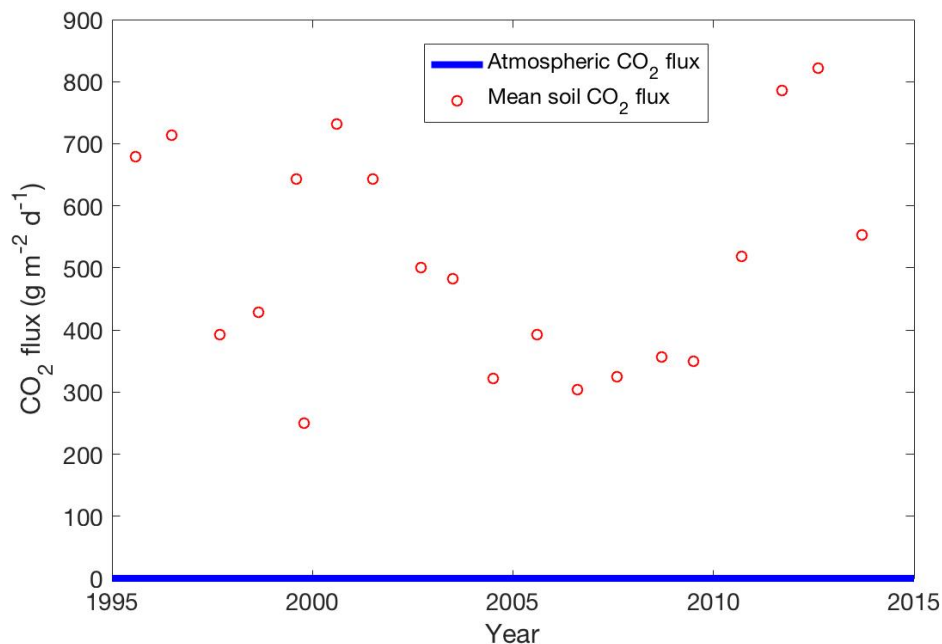


**Figure 1: The USGS has measured elevated soil CO<sub>2</sub> flux at Horseshoe Lake for the past two decades (Werner et al., 2014). These values are consistently higher than the atmospheric CO<sub>2</sub> measured by USGS California Volcano Observatory eddy covariance station at Horseshoe Lake at the time of AVIRIS overpass on October 21, 2014.**

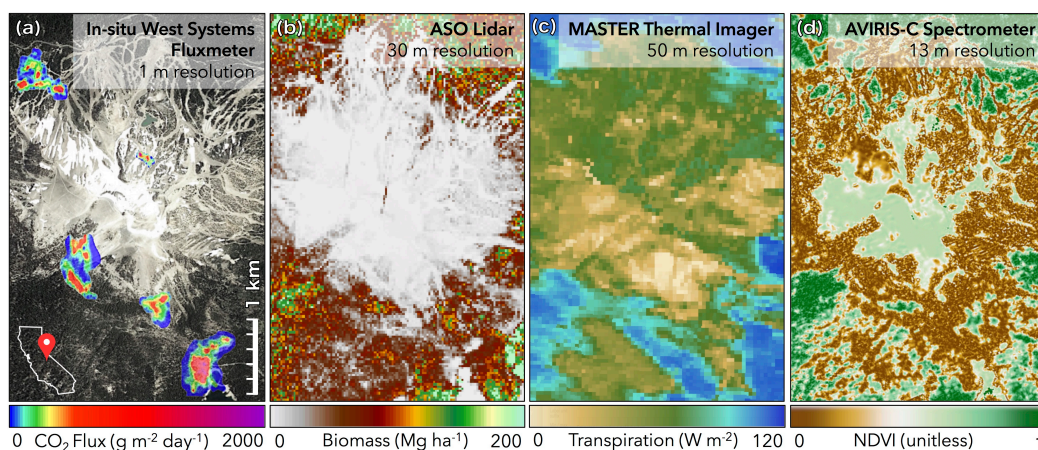


**Figure 2: A wealth of remotely sensed imagery has been acquired over Mammoth mountain. Some data products used in this study include (a) maps of soil CO<sub>2</sub> flux simulated based on accumulation chamber measurements, shown overlain on aerial RGB image; (b) above-ground biomass derived from Airborne Snow Observatory (ASO) lidar; (c) evapotranspiration derived from the MODIS/ASTER (MASTER) airborne simulator; and (d) Normalized Difference Vegetation Index (NDVI) derived from Airborne Visible/Infrared Imaging Spectrometer (AVIRIS image).**

10



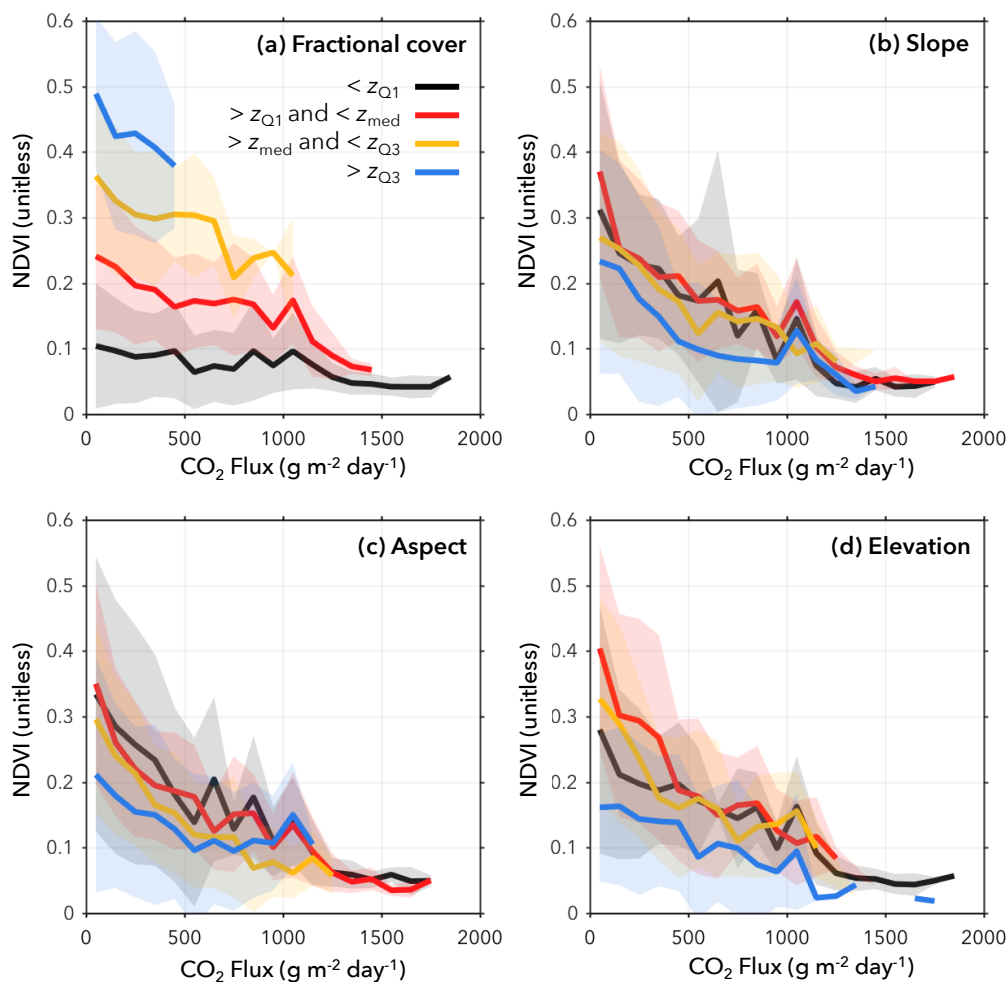
**Table 1:** Data sources are shown along with the year in which they were acquired, the original resolution of the dataset, and the method by which it was resampled. All datasets were resampled to the AVIRIS resolution of 13m.

<b>Data source</b>	<b>Year acquired</b>	<b>Original resolution</b>	<b>Resampling method</b>
Soil CO <sub>2</sub> flux	2011-2012	1 m	Nearest neighbour
Canopy height	2017	1 m	Nearest neighbour
Vegetation indices	2014	13 m	Original resolution
Foliar traits	2014	13 m	Original resolution
Fractional cover	2017	30 m	Nearest neighbour
Biomass	2017	30 m	Nearest neighbour
Evapotranspiration	2013	50 m	Nearest neighbour; Ma et al. resampling



**Table 2: The best performing vegetation indices (VI) and traits are shown with the predictive significance of eCO<sub>2</sub> in the model, and with their correlation with a regression ensemble that included elevation, slope, aspect, and fractional cover as confounding variables (n=5520). The most significant predictor was determined by ordering terms by p-values.**

Variable	Most significant predictor term	Estimate for eCO <sub>2</sub> coefficient	Standard error for eCO <sub>2</sub> coefficient	p-value for the eCO <sub>2</sub> term	Model R <sup>2</sup>
<i>Structure:</i>					
Canopy height	Slope, FC	6e-3	1e-3	4e-6	0.92
Biomass	FC	1e-1	2e-2	5e-6	0.83
<i>Composition (Vegetation indices):</i>					
Normalized Difference Vegetation Index (NDVI)	eCO <sub>2</sub>	-6e-5	8e-6	1e-12	0.68
Red Edge Normalized Difference VI	eCO <sub>2</sub>	-3e-5	6e-6	1e-9	0.67
Modified Red Edge Normalized Difference VI	eCO <sub>2</sub>	-7e-5	6e-6	2e-27	0.65
Vogelmann Red Edge Index 1	eCO <sub>2</sub>	-3e-5	1e-5	2e-3	0.64
Enhanced Vegetation Index	eCO <sub>2</sub>	-1e-4	1e-5	2e-22	0.62
Modified Red Edge Simple Ratio Index	FC	-1e-4	2e-5	5e-10	0.61
<i>Composition (Plant foliar traits):</i>					
Trait: Canopy nitrogen concentration	Intercept	-8e-3	1e-3	2e-7	0.45
Trait: Carbon	FC	3e-2	5e-3	5e-9	0.45
Trait: Leaf Mass per Area (LMA)	Aspect	3e-1	1e-1	6e-2	0.40
<i>Function:</i>					
Evapotranspiration (nearest neighbour)	FC	-8e-3	1e-3	5e-16	0.55
Evapotranspiration (statistical resampling)	FC	-3e-4	2e-3	8e-1	0.38



5 **Figure 3: Relationships between many ecological variables, including NDVI, and eCO<sub>2</sub> depend highly on confounding factors. The NDVI data is partitioned into quartiles and coloured such that, if  $z$  is the confounding variable (fractional cover, slope, aspect or elevation), then  $z_{Q1}$  is the first quartile of the confounding data;  $z_{med}$  is the median of the confounding data; and  $z_{Q3}$  is the third quartile. Partitioning by fractional cover yields clear separations in the response variable,**



as expected, since rising eCO<sub>2</sub> will have a less measurable effect on sparse vegetation within the pixel.

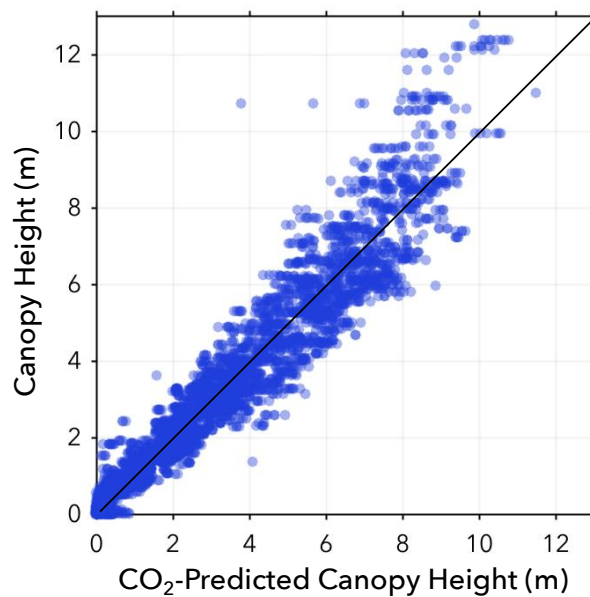
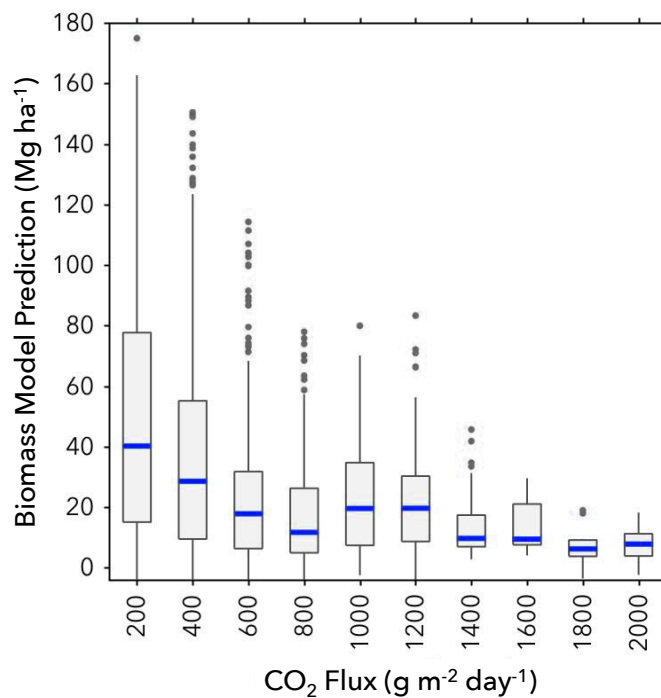
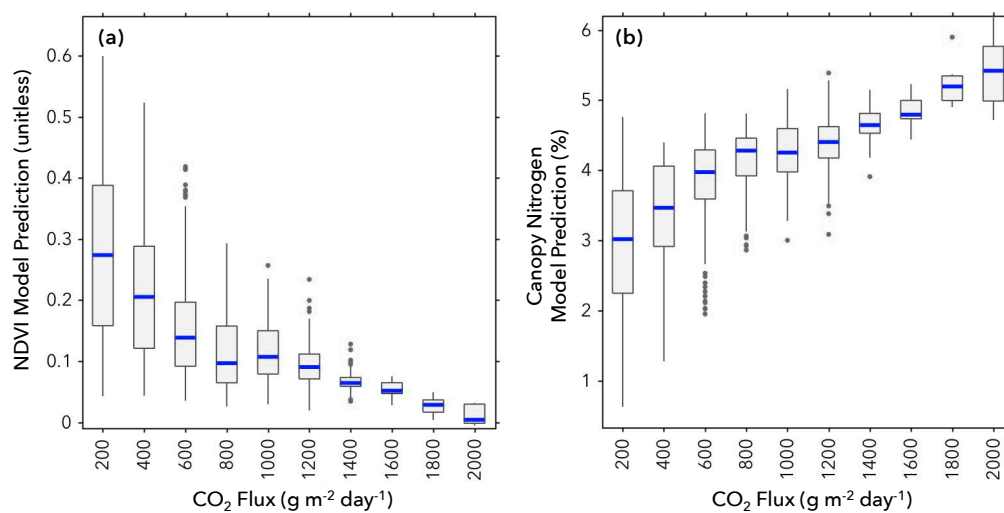


Figure 4: Canopy height is well modelled by the eCO<sub>2</sub> model, with an  $R^2=0.92$ , and the  
5 1-1 line shown in black. However, the very tallest trees are not well captured.



**Figure 5:** The biomass model prediction is shown for increasing eCO<sub>2</sub>. There is high variability at low eCO<sub>2</sub> values, but overall there is a small, but apparent, decrease in biomass with increasing eCO<sub>2</sub>.

5



**Figure 6: (a) The modelled NDVI prediction is shown for predictor variable  $e\text{CO}_2$ . There is a decrease in NDVI for increasing  $e\text{CO}_2$ , despite larger variance at low  $e\text{CO}_2$  values. (b) The modelled canopy nitrogen concentration trait prediction is shown for predictor variable  $e\text{CO}_2$ . There is a clear increase in canopy nitrogen concentration with increasing  $e\text{CO}_2$ .**

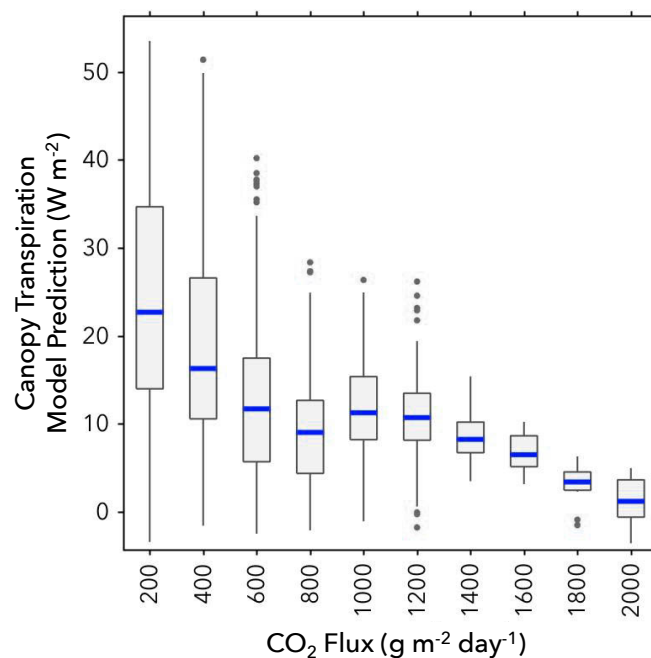


**Figure 7: The normalized canopy transpiration prediction is shown against predictor variable eCO<sub>2</sub>, for training data with nearest neighbour resampling. There is a clear decrease in ET for increasing eCO<sub>2</sub>, with larger variance at low eCO<sub>2</sub> values.**

5

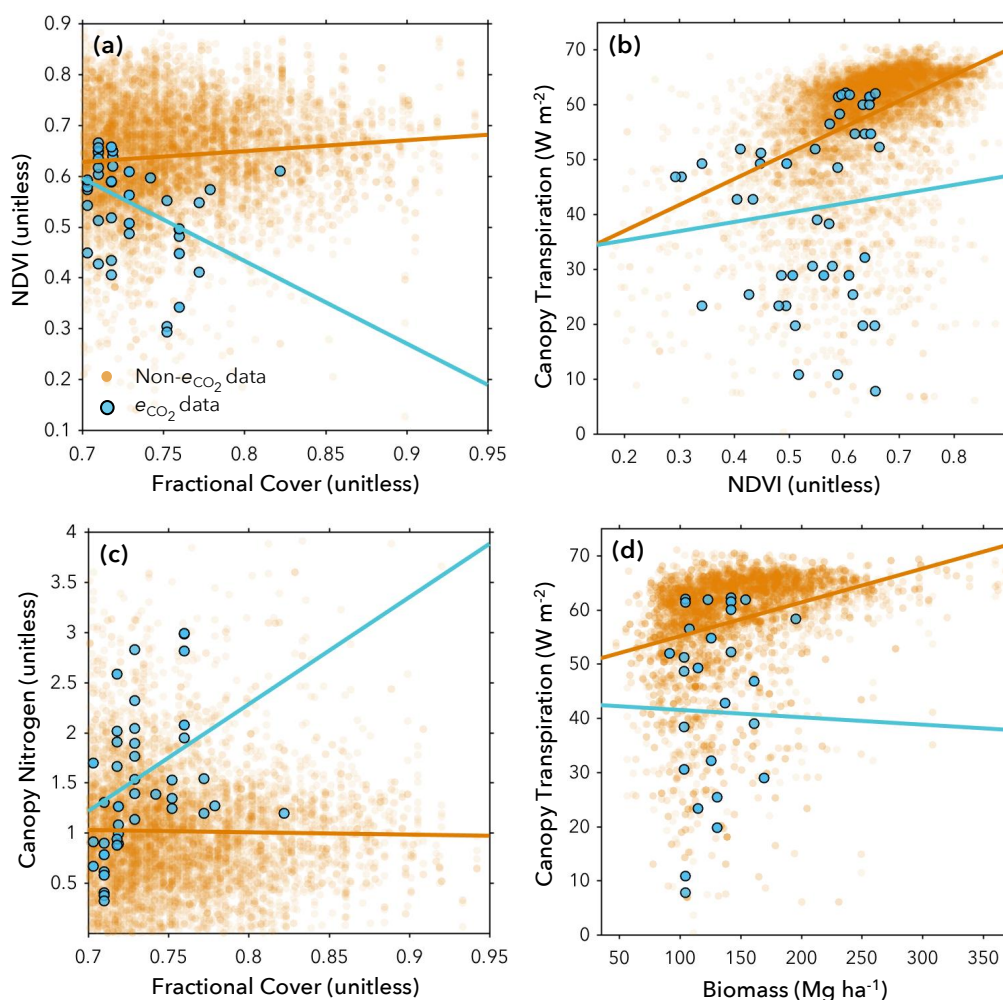


**Figure 8:** Ecosystem dynamics inside (blue data points) and outside (orange data points) of the eCO<sub>2</sub> measurement boundaries contrast. (a) In the entire image, NDVI increases slightly with increasing fractional cover. In the small eCO<sub>2</sub> subset, NDVI appears to decrease with increasing fractional cover. (b) In the entire image, evapotranspiration increases with increasing NDVI, whereas the small eCO<sub>2</sub> subset seems to cover points with lower ET. (c) Across the entire image, the nitrogen trait remains constant with increasing fractional cover (thresholded at FC>0.7). In the small eCO<sub>2</sub> subset, the nitrogen trait appears to increase with increasing fractional cover. (d) In the entire scene, evapotranspiration increases with increasing biomass. In the small eCO<sub>2</sub> subset, the evapotranspiration seems to be lower, on average, for the same range of biomass values.